DOI: 10.1002/ejic.200501140

High-Zirconium-Content Nano-Sized Bimodal Mesoporous Silicas

David Ortiz de Zárate,[a] Andrés Gómez-Moratalla,[a] Carmen Guillem,[a] Aurelio Beltrán,[a] Julio Latorre,[a] Daniel Beltrán,[a] and Pedro Amorós*[a]

Keywords: Mesoporous materials / Zirconia / Surfactants / Nanoparticles / Bimodal porous materials

Silica-based nanoparticulated bimodal mesoporous materials with high Zr content ($43 \geq Si/Zr \geq 4$) have been synthesized by a one-pot surfactant-assisted procedure from a hydroalcoholic medium using a cationic surfactant (CTMABr = cetyltrimethylammonium bromide) as structure-directing agent, and starting from molecular atrane complexes of Zr and Si as hydrolytic inorganic precursors. This preparative technique allows optimization of the dispersion of the Zr guest species in the silica walls. The bimodal mesoporous nature of the final high surface area nano-sized materials is confirmed by XRD, TEM, and N_2 adsorption–desorption isotherms. The small intraparticle mesopore system (with pore sizes around 2–3 nm) is due to the supramolecular templating effect of the surfactant, while the large mesopores (around 12–24 nm) have their origin in the packing voids generated by aggregation of the primary nanometric mesoporous particles. The basicity of the reaction medium seems to be a key parameter in the definition of this last pore system. The effects induced by the progressive incorporation of Zr atoms on the mesostructure have been examined, and the local environment of the Zr sites in the framework has been investigated by UV/Vis spectroscopy. Observations based on the consequences of post-treatments of the as-synthesized materials with HCl/ethanol mixtures corroborate that the atrane method leads to Zr-rich materials showing enhanced site accessibility and high chemical homogeneity throughout the pore walls.

Introduction

Silicon/zirconium mixed oxides, $(SiO_2)_{1-x}(ZrO_2)_x$, have attracted considerable attention for a long time because of their mechanical (low thermal-expansion coefficient) and chemical (resistance to alkaline attack) properties.[1–7] Moreover, they are also interesting materials in catalysis. Indeed, they exhibit catalytic activity due to both their moderate acidity and oxidizing capability, and also can be used as catalyst supports.[8] However, the possibility for industrial applications has been limited because these materials generally show low surface area and no size selectivity.[9,10] Hence, the search for improved-performance (high surface area) catalysts stimulated the preparation of $(SiO_2)_{1-x}(ZrO_2)_x$ solids in the form of particulated xerogels, which was approached through a diversity of sol-gel routes starting from alkoxide precursors.[11–13] The structure of these xerogels was studied some time ago by SAXS and WAXS techniques,[14] which revealed a very open architecture (involving interconnected 3D pore systems) that has been recently referred to as optimal for catalytic applications.[15] In practice, the $(SiO_2)_{1-x}(ZrO_2)_x$ particulated xerogels are high surface area catalysts displaying strong acidity and showing satisfactory activity in a diversity of organic reactions (cumene dealkylation, alcohol dehydration, alkene isomerization).[16–18]

However, the use of these $(SiO_2)_{1-x}(ZrO_2)_x$ xerogels as catalysts presents a certain limitation derived from their lack of size selectivity.[9,10] Until now, the most promising strategies to overcome this problem have been those conceived to incorporate Zr atoms into the frameworks of molecular sieves or high surface area silica-based materials.[19–21] Thus, there are reports on Zr-containing materials derived from both microporous solids (such as zeolites and also ALPOS)[22–25] and mesoporous silicas (Zr-MCM-41, Zr-MCM-48, Zr-HMS, Zr-MSU, Zr-SBA-15),[26–39] which simultaneously display high surface area and size selectivity. Hence, a diversity of both small and large substrates could be processed with the help of such a variety of Zr-containing molecular sieves.

In short, the preparative procedures implemented for incorporating zirconium in silica-based porous matrices can be referred to as one-pot (cohydrolysis) methods[26,32,34–36,38,39] or postsynthesis (grafting) treatments.[33,37] Independent of the synthesis strategy used, an important condition for having very active supported zirconia catalysts (high-Zr-content materials) lies in site isolation: the Zr atoms must be isolated and well dispersed throughout the silica walls, thus avoiding the formation of ZrO_2 domains.[40] In fact, while the preparation of doped mesoporous silicas is straightforward and usually leads to a relatively homogeneous distribution of cations, the situation changes when high dopant loads are required, and we must

[a] Institut de Ciència dels Materials (ICMUV), Universitat de València,
P. O. Box 2085, 46071 València, Spain
Fax: +34-96-3543633
E-mail: pedro.amoros@uv.es

face a complex chemistry plagued with problems, which often results in the absence of chemical homogeneity, phase segregation or mesostructure collapse.[41] Careful manipulation of the templating chemistry is thus required.

The origin of these problems lies in the different hydrolytic reactivity of elements such as Si and Zr (unequal hydrolysis and condensation reaction rates).[36,41] In practice, zirconium species usually hydrolyze faster than silicon precursors. In most cases, this results in partial segregation of ZrO_2 domains (together with a decrease of the Zr/Si molar ratio in the resulting mixed oxide with respect to the mother solution). Insofar as the catalysts' efficacy substantially depends on their purity and chemical homogeneity, phase segregation must be avoided. The goal of a variety of one-pot (cohydrolysis) synthesis procedures developed over the past few years was to circumvent this reactivity problem. Among the alternatives described, we can emphasize the utilization of Zr-complexing precursor species,[36,42] the use of single-source molecular precursors,[43] the optimization of the inorganic precursors and the pH,[44] the use of microwaves in the processing,[34] the application of hydrothermal post-treatments,[39] or chemical control based on adjusting the reaction conditions.[35] In this context, our group reported on how [using the atrane route,[45,46] that is to say starting from kinetically inert molecular atrane precursors (complexes of Si and Zr containing triethanolamine-derived ligands)] it is possible to orchestrate the Zr and Si hydrolytic reaction rates, thus leading to thermally stable Zr-MCM-41 porous silicas whose composition ranges from doped silicas to very-high-Zr-content materials ($\infty \geq Si/Zr \geq 0.3$).[36]

It should be emphasized that the main concern in these previous valuable investigations is the heteroelement (Zr) incorporation. Less attention has been paid to the site accessibility and connectivity in these silica-based catalysts, which also is a key for catalytic efficiency.[15] A strategy to deal with the site accessibility problem that recently has attracted interest is conceptually based on the consequences of decreasing the mesoporous particle size in the nanoparticle range.[15] This necessarily implies, at first, the shortening of the mesopore length, whereas the particle packing would generate supplementary interparticle porosity. The one-pot synthesis of functionalized (with inorganic elements and/or organic groups) nanoparticulated bimodal porous silicas was initially described by Pauly et al.[47] (Al-HMS materials) and El Haskouri et al.[48,49] (M-UVM-7 solids, M = Al, Ti, V, and Zr; HPNOs), who used in their processes a single surfactant (non-ionic, HMS; cationic, M-UVM-7, and HPNOs). In order to find applications, Pauly et al. demonstrated the benefits of this nanoparticle-based architecture by showing how the use of Al-HMS (average particle size < 200 nm) instead of Al-MCM-41 improves the yield in the catalytic alkylation of 2,4-di-*tert*-butylphenol with cinnamyl alcohol.[47] A two-step process for obtaining similar materials has recently been reported.[50] In any case, it must be noted that, until now, the heteroelement amounts which have been possible to incorporate into these nanoparticulated catalysts have not been too high (in the zirconia-supported materials we are dealing with, the upper limit was established at Si/Zr = 50 in ref.[48] vs. Si/Zr = 20 in ref.[50], although in this last case there is insufficient analytical information).

As mentioned in this Introduction, following previous work on related materials, we recently succeeded in synthesizing a novel family of nanoparticulated bimodal mesoporous pure and doped silicas, and published some of our preliminary results as a short communication.[48] On this basis, insofar as the interest on improved zirconia catalysts remains, we considered the possibility of transferring the mentioned nanoparticulated organization from the already explored limit of doped silicas up to the field of truly $(SiO_2)_{1-x}(ZrO_2)_x$ mixed oxides. We have succeeded in this aim, and this work describes the one-pot reproducible surfactant-assisted procedure that has allowed us to synthesize high-Zr-content nanoparticulated bimodal mesoporous silicas displaying high chemical homogeneity (good dispersion of the active sites) and a considerable amount of accessible Zr centers. The resulting Zr-UVM-7 solids bring together high heteroelement contents, the size selectivity provided by the surfactant-generated mesopores, and the high accessibility typical of xerogels. The effects of the presence of Zr atoms on the mesostructure have been examined, and the main features characterizing the Zr sites in the framework have been elucidated.

Results and Discussion

Synthesis Strategy

Bimodal mesoporous materials of the UVM-7 type that are rich in Zr atoms have been synthesized through a one-pot approach using CTABr as surfactant in a $TEAH_3$/water medium (CTABr = cetyltrimethylammonium bromide; $TEAH_3$ = triethanolamine) (see Exp. Sect.). Summarized in Table 1 are the main synthesis variables and physical data concerning the Zr-UVM-7 materials prepared in this way.

Our synthesis strategy has been designed both to overcome problems associated with the great reactivity differences that characterize the most usual Zr and Si precursor species (because of the lower electronegativity of Zr and its tendency to exhibit multiple coordination states) and to preserve, as far as possible, the nanoparticulated bimodal porous organization typical of UVM-7 silicas.[48] As mentioned above, this protocol is a modification of the so-called "atrane route", a simple preparative technique whose main points have been described previously in detail.[45] In fact, such a method has allowed us to successfully prepare a diversity of unimodal mesoporous single and mixed oxides, including the Zr-MCM-41 materials,[36] working under strongly basic conditions (pH = 11–12).[51–56] In contrast, in the case we are dealing with, the synthesis pH was buffered at ca. 9. It has been proven that these comparatively mild basic conditions favor the nucleation and growth of silica-based small nanoparticles,[48] thus avoiding the formation of relatively large particles typical of the MCM-41-like materials. In any case, the presence of atrane complexes

Table 1. Selected physicochemical properties of Zr-UVM-7 materials.

	Si/Zr		a_0	Δ_0	BET area	Pore size		Pore vol.		Wall thickness
	Gel	Solid[a]	[nm][b]	[nm][c]	[m^2/g]	Small pore [nm][d]	Large pore [nm][d]	Small pore [cm^3/g][d]	Large pore [cm^3/g][d]	[nm][e]
1	50	43	4.73	0.58	1146	2.99	24.2	1.03	1.58	1.74(2)
2	25	19	4.62	0.52	1036	2.80	14.6	0.83	0.99	1.82(2)
3	12	11	4.54	0.48	1001	2.75	12.1	0.79	0.66	1.79(2)
4	5	4	4.55	0.47	846	2.70	12.6	0.63	0.68	1.85(2)

[a] Si/Zr molar ratio in the porous samples estimated from EPMA. [b] Cell parameter calculated assuming a hexagonal cell [$a_0 = 2 \cdot d(100)/3^{1/2}$]. [c] Shrinkage after calcination (from XRD) defined as $\Delta_0 = a_0$(as-synthesized) – a_0(mesoporous). [d] Calculated from the adsorption branch of the isotherms and using the BJH model. [e] Pore wall thickness defined as a_0 – BJH small pore size.

in solution at the working pH, before and after water addition, has been confirmed by FAB-MAS. This study has been carried out firstly on independent Si- or Zr-containing solutions in which the reagent proportions are the same used in the preparation of the Zr-UVM-7 porous materials described in this work. In the absence of water, the majority species for both Si and Zr solutions correspond to M(TEA)-$(TEAH_2)$ [M = Si (100%) or Zr (100%)] monomers, and only in the Si case have additional entities been detected [$Si_2(TEA)_2TEAH$ and $Si_3(TEA)_4$], in very low proportions (12 and 15%, respectively). The relative intensities have been calculated without considering the peaks associated with the dissolvent. In contrast to previous experiments carried out at pH = 11,[36] the presence of oligomers is now practically negligible. Immediately after water addition, and independent of the pH ($9 < pH < 11$), both the Si and Zr atrane complexes remain in solution as monomers, $M(TEA)^+$ and M(TEA)OH (M = Si or Zr) being the majority hydrolyzed species. Later, the corresponding FAB signals progressively disappear as the sol evolves to gel. On the other hand, it must be emphasized that additional FAB-MAS experiments carried out on solutions containing both elements (Si and Zr) reveal (before and after water addition) the presence of the same species as in the independent solutions, which allows us to reasonably conclude that formation of binary (containing both Si and Zr entities) atrane complexes can be discarded. Thus, the precursor solution appears to mainly consist of a random intimate mixture of independent Zr and Si molecular monomeric fragments. In conclusion, although the proportion of oligomer species in the absence of water is dependent on the basicity of the medium, the use in the present case of moderately basic conditions (pH ≈ 9) to favor the formation of nanoparticulated materials does not seem to alter the nature of the Si and Zr species in hydroalcoholic solution (with regard to previous synthesis in more basic media). In other words, irrespective of the nature (condensation degree) of the starting atranes (pH-dependent), the hydrolyzed species become similar. In this way, the already studied role played by $TEAH_3$ in order to orchestrate the hydrolytic reactions of the Si and Zr precursor species[36] is preserved in the current synthesis of the Zr-UVM-7 solids. Finally, once the hydrolytic reactions have been completed, the total concentration of soluble silica can be accounted for by $Si(OH)_4$ and $(HO)_3SiO^-$ species in an approximate ratio of 10:1.6,[57,58] while the majority Zr species should be the $Zr(OH)_5^-$ monomer.[59] The subsequent condensation processes will proceed from these monomeric entities. In this sense, we can refer to a recent study on the condensation processes involving silicon and zirconium alkoxides, which demonstrates the formation of copolymerized tridimensional products in reaction media rich in water.[60] Then, the condensation processes of the hydrolyzed units must provide charged (anionic) binary (Si and Zr) oligomers that could match (by displacement of Br^- anions) with cationic surfactant aggregates [$(CTMA)_{mm}^+$] following an S^+I^- mechanism.

As mentioned above, the pH constitutes the key parameter to obtain nanoparticulated materials of this type. The working conditions (pH ≈ 9) have been selected in order to achieve high hydrolysis and condensation reaction rates and also low silica back solution.[57] Thus, silica polymerization is fastest at pH values in the range of 8–9, and the silica solubility reaches a minimum at pH ≈ 8.[57,58] Under these conditions, we favor (1) supersaturation, a necessary condition for the formation of a large number of small primary mesoporous nanoparticles, and (2) limited particle growth, as a consequence of the low silica solubility. Moreover, the incorporation of Zr helps to decrease the solubility. It is well known that the presence of heteroelements (such as Al or Zr) in the silica framework, even in low proportions, increases in a significant way the insolubility of the resulting doped or mixed oxides with regard to those of the respective individual oxides.[57] This property of Si/Zr mixed oxides has been exploited to prepare alkali-resistant filtration membranes based on mesoporous Zr-MCM-48 materials.[61]

Once the primary particles have been formed, the generation of a large pore system (see below) should be a consequence of their aggregation, which mainly implies the establishment of Si–O–Si interparticle covalent links (which might be kinetically favored in the presence of Zr^{IV}).[43] Moreover, as occurs in the case of xerogels, the presence of Zr favors the interparticle condensation reactions and leads to clusters more dense than those originated by the analogous pure silica derivatives.[14] This behavior may be attributed to the development of cross-linking through Zr centers between individual particles (Zr–O–Si or Zr–O–Zr bridges), as expected from the affinity of Zr atoms for higher oxygen coordination environments. Particle aggregation is a sol-gel process, which probably is the result of base-catalyzed interparticle collisions.[57] In short, the Zr incorporation into the silica walls helps to promote the nucleation of very insolu-

ble small nano-sized mesoporous particles, which in turn favors the stabilization of the UVM-7-like organization.

Characterization

We have used EPMA both to determine the real amounts of Zr incorporated into the framework and also to check the chemical homogeneity of the resulting solids [a relevant objective of our work was to preserve, under the new working conditions, good dispersion of the heteroelement (Zr) in the walls of the resulting materials, which usually is achieved through the atrane route]. Summarized in Table 1 are the corresponding Si/Zr molar ratio values (averaged from data of about 50 different particles) of the resulting solids. EPMA shows that the reported Zr-UVM-7 materials contain Si/Zr molar ratios similar to those present in the mother solutions. This fact indicates that, in general, there is no preferential incorporation of Zr or Si into the final porous walls. However, we observe a certain increase of the Zr proportion in the case of the solids prepared from the precursor solutions having the lowest Zr contents (Si/Zr = 50 and 25). This result could be associated with the comparatively low solubility of the Zr-containing species (with regard to the pure silica ones), the effect of which should decrease as the amount of well-dispersed Zr centers increases. On the other hand, EPMA also shows that all Zr-UVM-7 samples are chemically homogeneous (have regular distributions of Zr and Si atoms) at the micrometer level (spot area $\approx$ 1 μm) with a constant and well-defined composition. Hence, the Zr-UVM-7 solids can be considered as monophasic products. In fact, segregation of extra-framework crystalline ZrO_2 can be practically discarded even for the samples having the highest Zr content (although formation of ZrO_2-like amorphous nanodomains might progress as the Zr content increases). This result is consistent with the absence of zirconia peaks in the high-angle region of the XRD patterns. In short, according to our initial hypothesis, we can conclude that the use of atrane precursors results in the harmonization of the rates of the hydrolytic processes involving the corresponding Si and Zr species, which facilitates the incorporation of relatively high amounts of the heteroelement (Zr). Indeed, the amounts of Zr which are incorporated into Zr-UVM-7 solids are higher than those usually achieved in other related silica-based materials prepared from conventional Si and Zr sources (for a given Si/Zr initial ratio). Even more, as mentioned above, the use of the atrane route allows very-high-Zr-content porous silicas to be obtained, but the nanoparticulated organization of the material we are looking for is lost when the Si/Zr molar ratio becomes smaller than 4:1.

The TEM images in Figure 1 clearly show that the UVM-7-like organization is maintained in the compositional range of 43 $\geq$ Si/Zr $\geq$ 4. All solids present a continuous nanometric array constructed from aggregates of nano-sized mesoporous particles, which include two different pore systems: (1) the first one can be related to the porogen effect of the surfactant-templating micelles, which generates the small intraparticle regular mesopores organized in a short-range hexagonal-ordering array, and (2) the second one consists of large cage-like interparticle pores and corresponds to the voids appearing as a consequence of the collision and aggregation of the primary nanoparticles. According to its origin, this second pore system presents a nonordered character similar to that defining the cross-linked network in nanoparticulated xerogels.[62,63]

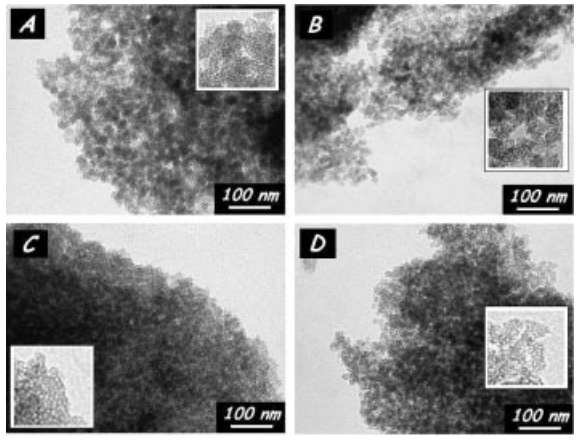

Figure 1. Representative TEM images of Zr-UVM-7 materials: (A) Sample 1 (Si/Zr = 43), (B) Sample 2 (Si/Zr = 19), (C) Sample 3 (Si/Zr = 11), and (D) Sample 4 (Si/Zr = 4). The insets show enlarged (×3) TEM images.

On the other hand, a careful analysis of the TEM images allows certain tendencies in the variation of both the particle morphology and the progress of the cluster-like aggregation with the Zr content to be established. Thus, the average particle size slightly decreases as the Zr content increases. The progressive Zr incorporation also favors the formation of denser aggregates, reflecting a more efficient packing of the primary nanoparticles. Such an evolution of the mesostructure can be firstly related to the solubility decrease induced by the Zr incorporation. Thus, the particle growth decreases as the insolubility of the nanoparticles increases. Moreover, the ability of Zr atoms to increase their coordination number favors the interparticle connectivity (based on Si–O–Si covalent bonds) through (additional) Zr–O–Zr or Zr–O–Si links. This results in an interparticle shrinkage similar to that observed in xerogels.[14] These tendencies can be better appreciated by comparing a pure UVM-7 silica with a Zr-containing derivative (Figure 2). The micrographs in Figure 2 clearly show how the incorporation of Zr atoms also involves a change in the particle morphology. Indeed, while the UVM-7 pure silica exhibits aggregates defined by regular elliptical nanoparticles, these primary building blocks in the Zr-UVM-7 materials present an irregular and angular shape. It is well known that, independently of the particle size (nano- or micrometric Stöber-like silica particles), the incorporation of Zr (or another heteroelement) strongly affects the regular growth of the silica spheres, thus leading to irregular particles. A similar morphologic evolution with the Zr content was described previously for Zr-containing silica xerogels.[14]

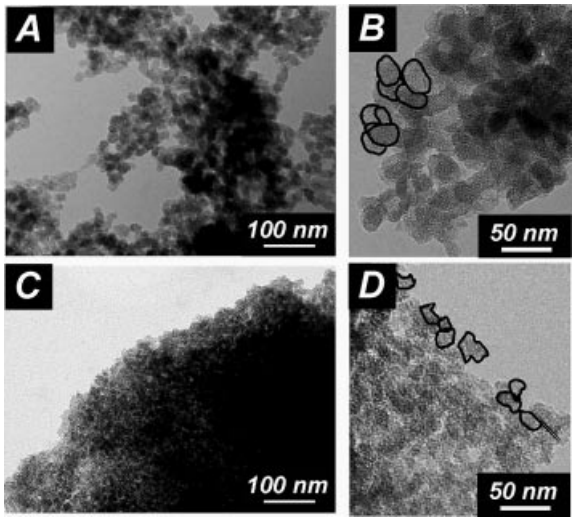

Figure 2. Comparative TEM micrographs of (Zr-free) UVM-7 silica (A and B) and Zr-UVM-7 Sample 3 (C and D).

The characteristics of the intraparticle mesopore array have been further studied by XRD with results that fully correlate to TEM observations. All materials (as-synthesized and calcined) display XRD patterns with at least one strong diffraction peak in the low-angle region, which is characteristic of mesostructured solids. The low-angle region of the XRD patterns corresponding to the mesoporous (calcined) samples is shown in Figure 3. In all these last cases, apart from the intense peak at low 2θ values [associated with the (100) reflection if a basic hexagonal cell is assumed],[64] we can observe a broad signal of relatively low intensity that can be indexed to the overlapped (110) and (200) reflections of the typical hexagonal cell. The observation of this last unresolved broad signal is characteristic of an MCM-41-like short-range hexagonal intraparticle mesopore topology. We can also notice the decrease of the relative intensity of this broad signal with the Zr content (it appears as a shoulder on the main peak for samples in which Si/Zr $\leq$ 19). Such an evolution is indicative of a progressive lowering of order in the mesopore array as the Zr amount incorporated into the silica walls increases. The lattice parameter value remains practically unchanged in the range of 43 $\geq$ Si/Zr $\geq$ 4 for both the as-synthesized (about 5.20 ± 0.13 nm) and porous (about 4.64 ± 0.10 nm) materials. Assuming the effective incorporation of Zr atoms in the silica framework, this result might seem a priori unreasonable [even more so when compared to the values of the a_0 parameter of the mesostructured (5.13 nm) and calcined (4.91 nm) UVM-7 pure silica]. To understand this behavior, it is necessary to consider two opposite phenomena: (1) cell expansion due to the replacement of Si atoms with Zr ones, and (2) strong intraparticle network-shrinkage associated with the cross-linking ability of Zr, which is enhanced after calcination. As shown in Table 1, the contraction of the a_0 parameter upon calcination for the Zr-containing materials (about 0.51 ± 0.07 nm) is significantly higher than that observed for the Zr-free UVM-7 silica (0.22 nm).[65] It must be emphasized that this significant shrinkage is similar to those observed in the cases of Zr-MCM-41[36] and (pure) ZrO_2[66] mesoporous solids prepared through surfactant-assisted procedures.

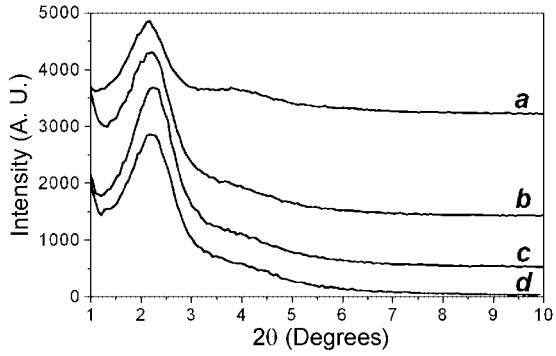

Figure 3. Low-angle XRD patterns of Zr-UVM-7 materials: (a) Sample 1 (Si/Zr = 43), (b) Sample 2 (Si/Zr = 19), (c) Sample 3 (Si/Zr = 11), and (d) Sample 4 (Si/Zr = 4).

The N_2 adsorption–desorption isotherms gathered in Figure 4 corroborate that the bimodal pore system typical of nanoparticulated UVM-7 silicas is maintained in the Zr-UVM-7 (43 $\geq$ Si/Zr $\geq$ 4) materials. The curves show, in all cases, two well-defined adsorption steps (at intermediate and high partial pressures). The adsorption at P/P_0 values in the range of 0.25–0.50 can be related to capillary condensation of nitrogen inside the cylindrical intraparticle surfactant-templated mesopores. The second adsorption at $P/P_0 > 0.65$ corresponds to the filling of the large cage-like interparticle voids. Application of the BJH model (see Figure 5) allows independent analysis of the evolution with the Zr content of the two pore systems.

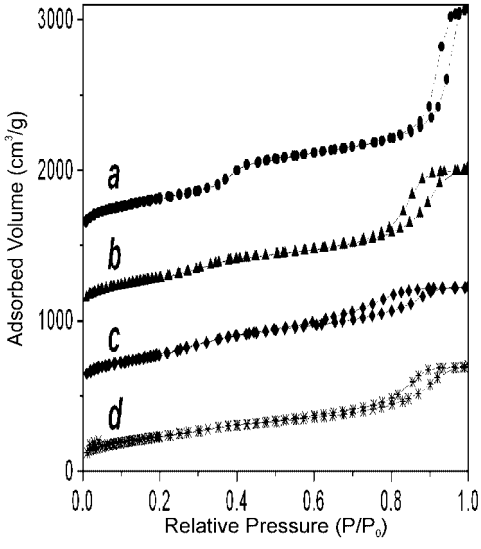

Figure 4. N_2 adsorption–desorption isotherms for Zr-UVM-7 materials: (a) Sample 1 (Si/Zr = 43), (b) Sample 2 (Si/Zr = 19), (c) Sample 3 (Si/Zr = 11), and (d) Sample 4 (Si/Zr = 4).

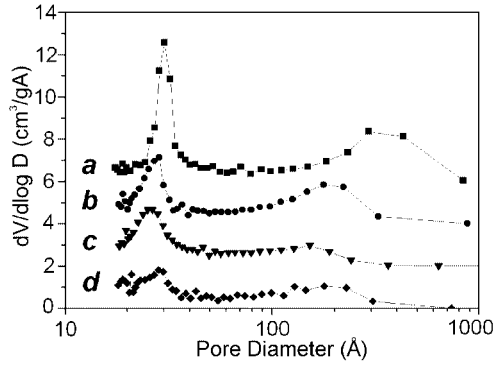

Figure 5. BJH pore size distributions for Zr-UVM-7 materials: (a) Sample 1 (Si/Zr = 43), (b) Sample 2 (Si/Zr = 19), (c) Sample 3 (Si/Zr = 11), and (d) Sample 4 (Si/Zr = 4).

Indeed, the pore size and volume associated with the intraparticle small mesopores gradually decrease with the Zr content (see Table 1), a result which is consistent with an effective heteroelement incorporation into the silica walls. The intraparticle shrinkage commented on above could account for such a BJH pore and volume evolution. On the other hand, we observe similar tendencies for the pore size and volume associated with the interparticle pores in the case of oxides (doped or mixed) with intermediate Zr loads ($43 \geq Si/Zr > 11$). Later, as the Zr content increases ($11 \geq Si/Zr \geq 4$), the pore size and volume seem to be stabilized. At this point, it can be interesting to compare these results with those concerning the interparticle pore system (pore size = 50–60 nm) corresponding to pure (Zr-free) UVM-7 silicas.[48] We can conclude that Zr centers seem to be very effective for interconnecting different nanoparticles (with the consequent pore-size reduction) even for low heteroelement contents. Thus, the incorporation of small amounts of Zr (Si/Zr = 43) already implies a reduction of the large pore size in about 50% with regard to the pure UVM-7 silica. This reduction continues more smoothly until significant Zr contents ($Si/Zr \geq 11$) are reached, for which we might consider that the size and volume of the interparticle pore system is roughly stabilized (about 12.5 nm and 0.67 cm^3/g). This general behavior suggests that, in the presence of moderate proportions of interparticle Zr binding sites, the cage-like pore system is controlled by the nanoparticle packing efficiency (physical aspects related to the size and shape of the particles) rather than by the heteroelement amount.

The high BET surface area, characteristic of UVM-7 and MCM-41 materials, is maintained in the whole compositional range studied (Table 1). Incorporation of Zr leads to a small and gradual decrease of the BET area. Insofar as the major surface area corresponds to the intraparticle mesopore system, this evolution must be attributed to disorder induced by Zr in the surfactant-templated pore array. This is a general tendency already observed for M-MCM-41-like samples,[38] which has to be related to the relative lowering of the S^+I^--matching capability of the heteroelement-containing silica oligomers. However, this BET surface area decrease does not necessarily imply a significant loss of porosity, and it could be related to a great extent with the gradual increase of the density of the samples as Zr atoms replace Si ones. Also, the thickness of the pore walls (defined as $Wt = a_0$ – BJH pore size) shows a certain tendency to increase with the Zr content, which should be correlated with the effective incorporation of Zr into the walls.

Once it is unambiguously confirmed that our materials retain the nanometric architecture typical of the UVM-7 silicas, it is possible to gain insight into the characteristics of the local environment and dispersion of the Zr centers in the silica walls with the help of UV/Vis spectroscopy. The diffuse-reflectance UV/Vis spectra corresponding to the anhydrous (i) and hydrated (ii) Zr-UVM-7 compositions we are dealing with (the spectrum of bulk ZrO_2 has also been included for comparative purposes) are shown in Figure 6.

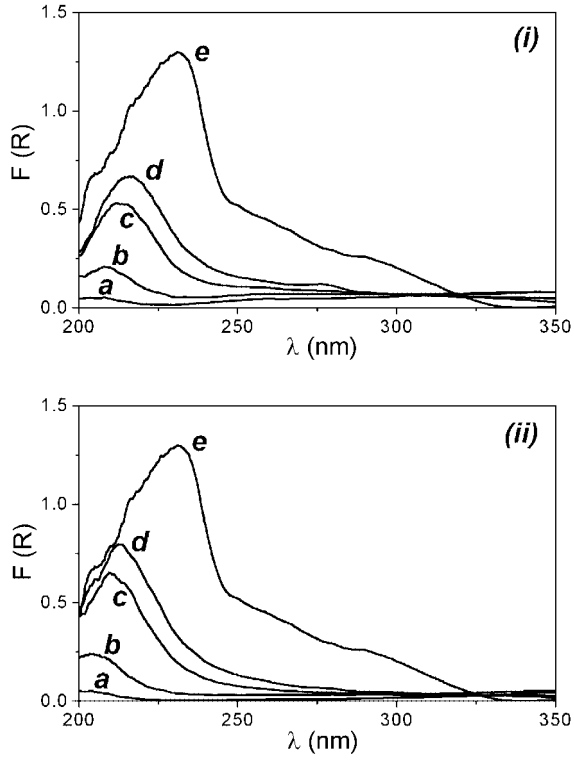

Figure 6. Diffuse-reflectance UV/Vis spectra of (i) anhydrous and (ii) hydrated Zr-UVM-7 samples. (a) Sample 1 (Si/Zr = 43), (b) Sample 2 (Si/Zr = 19), (c) Sample 3 (Si/Zr = 11), (d) Sample 4 (Si/Zr = 4), and (e) ZrO_2.

In all cases, the spectra display an intense absorption band at about 210–217 nm whose intensity monotonically increases as the Si/Zr ratio decreases. As can be seen, the spectrum of ZrO_2 is clearly different: the most intense absorption band is complex and its maximum appears at comparatively low energy values (about 230–240 nm); moreover it exhibits additional bands in the range of 250–350 nm. The intense adsorption band in the spectra of Zr-UVM-7-related materials is usually attributed to ligand-to-metal charge transfer from oxide entities to isolated Zr^{IV} cations in a tetrahedral environment.[67] This band presents a gradual red-shift as the Zr content increases, but the absorption maximum always falls at wavelengths lower than that corre-

sponding to pure zirconia, that is to say the band-gap energies for the Zr-UVM-7 materials are larger than for ZrO_2.[68] This result further corroborates the lack of extra-framework bulk ZrO_2 as a segregate phase in the Zr-UVM-7 samples, and also indicates the presence of isolated Zr centers (or highly dispersed zirconia-based clusters or nanodomains) in the pore walls. FTIR spectroscopic data offer further evidence in this sense. Thus, the relative intensity of the band at ca. 970 cm^{-1}, which is usually related to vibrational modes involving Si–O–Zr linkages,[69] clearly increases with the Zr content. Moreover, the detection of a certain UV/Vis absorption in the range of 250–350 nm has been recognized as characteristic of nanoscopic regions containing Zr–O–Zr bonds in related materials.[34] It must be noted that the spectrum of bulk ZrO_2 presents, at least, two rather intense adsorption bands in this range. In the case of the Zr-UVM-7 solids, we cannot detect any absorption in this spectral range until reaching the Zr content corresponding to a molar ratio of Si/Zr = 11. Even in the case of the spectrum of the highest-Zr-content material (Si/Zr = 4), we can observe only a small shoulder at ca. 250–275 nm. We cannot disregard, therefore, the presence of a certain proportion of Zr–O–Zr-containing nanodomains in this last sample of high Zr content. Such a shoulder can be better appreciated in the spectrum of the anhydrous Si/Zr = 4 sample. The thermal treatment carried out to eliminate water probably favors a certain intra- and interparticle condensation leading to the formation of new Zr–O–Zr bonds. As discussed above, this observation correlates to the ability of Zr centers to adopt different coordination environments.

Concerning the potential catalytic applications of these materials, it seems relevant to evaluate the proportion of Zr sites that are reagent-accessible. In general, this variable is highly dependent on the synthesis approach used. Thus, when comparing cohydrolysis processes to grafting techniques, we find that, although cohydrolysis usually leads to higher chemical homogeneity, it has an associated drawback: the loss of a significant part of the incorporated, potentially active centers, which are buried inside the pore walls (that is to say inaccessible for the reagents). Then, assuming that the mesoscopic organization of the material is maintained, we can consider that only those Zr centers close to the pore surface should be accessible to different substrates. Our approach to estimating the proportion of Zr-accessible sites in the Zr-UVM-7 materials is based on evaluating the effects of using an alternative procedure for removing the surfactant from the as-synthesized samples. Thus, we chemically extracted the surfactant with the help of HCl/ethanol mixtures. This process has a double effect: it obviously provokes the exchange between $CTMA^+$ species and protons, but also favors the leaching of accessible Zr atoms in the form of chloride complexes. Thus, we observe in all cases that the Zr content, as measured by EPMA, decreases after extraction (see Table 2).

In all samples, at least 1/3 of the Zr centers are accessible under the experimental conditions we have used. Moreover, the proportion of accessible Zr centers increases with the Zr content [from about 40% (Si/Zr = 43) to about 60% (Si/Zr = 4)]. At first glance, this evolution might suggest that there is a certain progressive (with the Zr content) loss of chemical homogeneity of the pore walls, which would result in enrichment in Zr of the surface with regard to the core walls. However, these results must be carefully considered, because the leaching of superficial Zr centers (or ZrO_2 nanodomains in the Zr-richest samples) also favors a progressive attack on partially buried Zr species. In practice, this degradation will progress continuously, leading to an enhanced elimination of Zr (internal and a priori inaccessible) cations of the inorganic walls. This process really is very similar to the well-known dealumination and desilication reactions carried out on zeolites to favor the generation of additional hierarchical porosity.[70,71] A possible consequence of the progressive formation of new disordered pores should be mesostructure degradation (partial or total). In fact, a preliminary study (XRD and N_2 adsorption–desorption) carried out on chemically extracted samples shows that the process induces significant changes in the (UVM-7) organization of the resulting materials. Thus, according to the XRD patterns in Figure 7, the intraparticle short-range hexagonal ordering mesopore system is maintained only up to Sample 3 (initial molar ratio: Si/Zr = 11), and it practically disappears for the Zr-richest material (Sample 4).

Table 2. Analytical data for Zr-UVM-7 samples before and after treatment with HCl/ethanol.

Sample	Si/Zr calcined	Si/Zr chemically extracted	Accessible Zr sites (%)
1	43	66	35
2	19	34	41
3	11	24	50
4	4	11	60

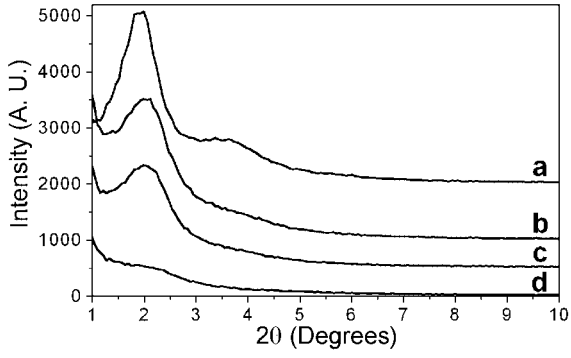

Figure 7. Low-angle XRD patterns of the chemically extracted Zr-UVM-7 materials: (a) Sample 1 (Si/Zr = 66), (b) Sample 2 (Si/Zr = 34), (c) Sample 3 (Si/Zr = 24), and (d) Sample 4 (Si/Zr = 11).

On the other hand, we only observe (see Figure 8) UVM-7-like isotherms (with two well-differentiated adsorption steps) up to Sample 2 (initial molar ratio: Si/Zr = 19). Indeed, as the Zr content increases, the first adsorption step (associated with the intraparticle mesopores) progressively disappears, and the second adsorption step (typical of interparticle voids) in the isotherms evolves to wide pore-size distributions.

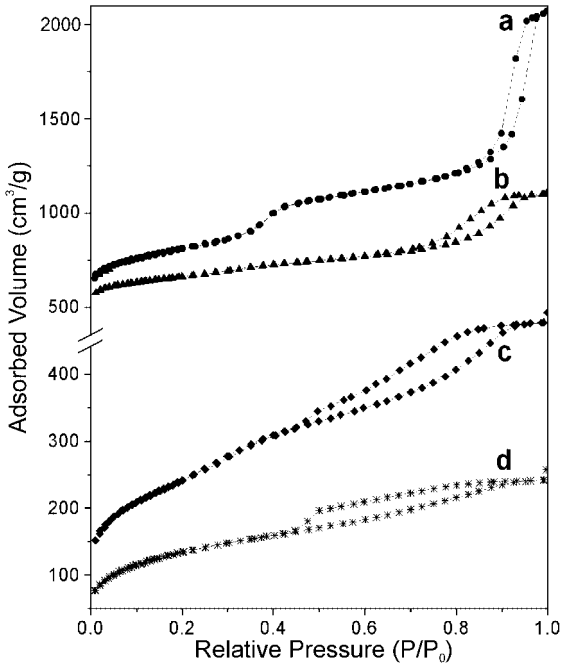

Figure 8. N_2 adsorption–desorption isotherms of the chemically extracted Zr-UVM-7 materials: (a) Sample 1 (Si/Zr = 66), (b) Sample 2 (Si/Zr = 34), (c) Sample 3 (Si/Zr = 24), and (d) Sample 4 (Si/Zr = 11).

According to XRD and porosimetry data, we can conclude that the UVM-7-like architecture in chemically extracted materials is preserved only in the compositional range of $43 \geq Si/Zr > 19$ (initial molar ratio values). On the basis of this observation, and taking into account both the proportion of accessible Zr sites estimated for the samples in this range (from 35 to 40%, Table 2) and their wall thickness (Table 1), it is possible to propose a rough structural model for estimating the degree of chemical homogeneity of the pore walls. Then, assuming the existence of a silica-based framework constructed from Q^4 centers [*d*(Si–O) = 0.16 nm], about six silica chains are necessary to achieve a wall thickness of ca. 1.7–1.8 nm (Figure 9). Under the reasonable hypothesis that in the low-Zr-content silicas ($Si/Zr > 19$) only the Zr sites located in the more external chains should be eliminated by the treatment with HCl/ethanol mixtures, the proportion of accessible Zr centers for a homogeneous heteroelement dispersion is 1/3, a value very close to those observed for Samples 1 and 2 (35% and 41%, respectively). In any case, although a slight Zr surface enrichment cannot be completely disregarded, we can conclude that the atrane method leads to mesoporous materials with high chemical homogeneity throughout the pore walls. In contrast, an appreciable Zr enrichment of the surface has been detected for mesoporous materials synthesized from conventional reagents.[35] Dealing with the surfactant-exchanged materials in the compositional range of $11 \geq Si/Zr > 4$, it is interesting to point out that, as occurs for zeolites, the gradual degradation of the mesostructure by Zr leaching to induce additional hierarchic porosity may be controlled to increase the material accessibility. In this regard, additional work is currently in progress.

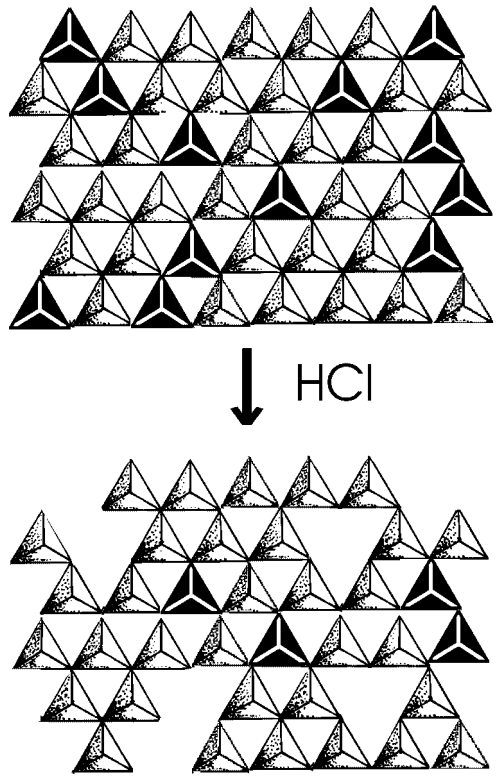

Figure 9. Scheme of the pore wall. Grey and white positions in the framework correspond to Zr and Si sites, respectively.

Conclusions

In short, we reported here on how, starting from kinetically inert atrane precursors, it is possible to synthesize high-zirconium-content nano-sized bimodal porous silicas by using a cationic surfactant-assisted procedure under controlled pH conditions. The resulting Zr-UVM-7 silica-based materials maintain the typical array of the parent pure silica: aggregates of nano-sized mesoporous particles defining a large interparticle pore system resulting from the imperfect packing of the primary building blocks. The effects of the Zr atoms on the UVM-7 pore morphology are explained on the basis of both the modification of the silica solubility by incorporation of Zr centers into the oligomers and the ability of the Zr atoms to expand their coordination number. The latter aspect favors a significant decrease of the textural porosity with regard to Zr-free UVM-7 materials. Once more, the atrane method proves to be a very efficient tool to achieve a good dispersion of the heteroelement guest species in the silica framework.

Experimental Section

Chemicals: All the synthesis reagents were analytically pure, and were used as received from Aldrich. The Si and Zr primary sources were tetraethyl orthosilicate (TEOS) and zirconium isopropoxide

(ZrP), respectively. 2,2′,2′′-Nitrilotriethanol or triethanolamine [$N(CH_2–CH_2–OH)_3$, $TEAH_3$] was used for obtaining Si and Zr atrane complexes. The templating agent was cetyltrimethylammonium bromide (CTMABr).

Synthesis: The method was a modification of the so-called "atrane route".[36,45,46] The nano-sized Zr-UVM-7 materials were synthesized through a one-pot surfactant-assisted procedure in a homogeneous hydroalcoholic reaction medium (water/$TEAH_3$). The cationic surfactant (CTMABr) acted as a structure-directing agent or supramolecular template (and consequently, as porogen after template extraction). Although the Si and Zr primary sources were commercial alkoxides, the real hydrolytic precursors in this strategy were Si and Zr atranes (relatively inert complexes that include $TEAH_3$-related ligand species).[36,45,46] Together with its complexing ability, the presence of the polyalcohol ($TEAH_3$) was a key because it kept the reaction medium buffered (pH ≈ 9), favoring the formation of nanoparticulated materials.[47,48] Details of a typical synthesis leading to Sample 2 (see Table 1) can be described as follows: (1) Preparation of an adequate mixture of atrane precursors from commercial alkoxides. TEOS (32.1 mL, 0.144 mol) and ZrP (2.56 mL of a 70% in weight solution, 0.0058 mol) were slowly added to liquid $TEAH_3$ (66.9 mL, 0.51 mol) and heated at 150 °C to give atrane complexes. (2) Addition of the structure-directing (porogen) agent. After cooling of the previous solution to 90 °C, CTMABr surfactant (13.68 g, 0.0375 mol) was added. (3) Mesostructure formation. The solution containing the atrane complexes and the template was cooled to 60 °C and mixed with water (240 mL, 13.33 mol). After a few seconds, a white powder appeared. The resulting suspension was allowed to age at room temperature for 24 h. The final (mesostructured) powder was filtered off, washed with water and ethanol, and air-dried. (4) Surfactant removal. In order to open the pore system, the as-synthesized solid was heated at 500 °C under static air for 5 h. In all cases, the molar ratio of the reagents in the mother liquor was adjusted to (2–x)Si/xZr/7$TEAH_3$/0.52CTMABr/180H_2O (where x = 0.04, 0.08, 0.15, and 0.33). On the other hand, in order to evaluate the proportion of internal and external (accessible) Zr sites, we used an alternative procedure to remove the surfactant from the as-synthesized samples. Indeed, the surfactant was chemically extracted from some selected samples using an HCl/ethanol solution (about 1 g of powder, 15 mL of HCl 35%, and 150 mL of ethanol 96%) by maintaining the suspension of the mesostructured solid in the solution, while stirring at room temperature for 24 h. The final (porous) material was separated by filtration, washed with ethanol, and air-dried.

Physical Measurements: All solids were characterized by electron probe microanalysis (EPMA) using a Philips SEM-515 instrument. The Si/Zr molar ratio values averaged from EPMA data corresponding to about 50 different particles of each sample are summarized in Table 1. Fast atomic bombardment (FAB) coupled to mass spectrometry (MAS) analysis of the precursor solutions was performed to investigate the nature of the atrane precursors (before and after water addition). X-ray powder diffraction (XRD) data were recorded with a Seifert 3000TT θ-θ diffractometer using Cu-K_α radiation. Low-angle XRD patterns were collected in steps of 0.02° (2θ) over the angular range of 0.65–10° (2θ) for 25 s/step. To detect the presence of some crystalline bulk phase, additional patterns were recorded with a larger scanning step [0.05° (2θ)] over the angular range of 10–70° (2θ) and a lower acquisition time (10 s/step). An electron microscopy study (TEM) was carried out with a JEOL JEM-1010 instrument operating at 100 kV and equipped with a CCD camera. The specimens for TEM analysis were prepared from powders by conventional crushing in an agate mortar, and dispersing the resulting small crystallites in dodecane. Microparticles were then deposited on holey carbon microgrids under ambient conditions. Surface area, pore size, and volume values were calculated from nitrogen adsorption–desorption isotherms (–196 °C) recorded with a Micromeritics ASAP-2010 instrument. Calcined samples were degassed at 130 °C and 10^{-6} Torr for 15 h prior to measurement. Surface areas were estimated according to the BET model,[72] and pore size dimensions were calculated by using the BJH method (measures at $P/P_0 < 0.55$ and $P/P_0 > 0.55$ values have been used to characterize the intrananoparticle and the internanoparticle pore systems, respectively).[73] Room-temperature diffuse-reflectance spectra were registered using a Shimadzu UV/Vis 2501PC instrument equipped with an integrated sphere coated with $BaSO_4$, which also is used as standard. IR spectra (KBr pellets) were registered with an FTIR Perkin–Elmer 1750 spectrophotometer.

Acknowledgments

This work was supported by the Spanish Ministerio de Educación y Ciencia (under grants MAT2002-04329-C03-02 and MAT2003-08568-C03-01) and the Generalitat Valenciana (grant GRUPOS03/099 and GV2004-B-745). D. O. Z. thanks the Spanish Ministerio de Educación y Ciencia for a doctoral grant.

[1] R. C. Garvie, R. H. Hannik, R. T. Pascoe, *Nature* **1975**, *258*, 703–704.
[2] A. Paul, *Chemistry of Glasses*, Chapman and Hall, London, **1982**.
[3] M. Nogami, M. Tomozawa, *J. Am. Ceram. Soc.* **1986**, *69*, 99–102.
[4] M. Palladino, F. Pirini, M. Beghi, P. Chirulo, G. Cogliati, L. Costa, *J. Non-Cryst. Solids* **1992**, *147–148*, 335–339.
[5] F. Garbassi, L. Balducci, R. Ungarelli, *J. Non-Cryst. Solids* **1998**, *223*, 190–199.
[6] T. Lopez, F. Tzompantzi, J. Navarrete, R. Gomez, J. L. Boldu, E. Muñoz, O. Novaro, *J. Catal.* **1999**, *181*, 285–293.
[7] H. Yang, R. Lu, L. Shen, L. Song, J. Zhao, Z. Wang, W. Li, *Mater. Lett.* **2003**, *57*, 2572–2579.
[8] K. Tanabe, M. Misono, Y. Ono, H. Hattori, *Stud. Surf. Sci. Catal.* **1989**, *51*, 1–5.
[9] K. Tanabe, T. Yamaguchi, *Catal. Today* **1994**, *20*, 185–198.
[10] T. Yamaguchi, *Catal. Today* **1994**, *20*, 199–218.
[11] R. Takahashi, K. Nakanishi, N. Soga, *J. Ceram. Soc. Jpn.* **1998**, *106*, 772–777.
[12] H. Hayashi, H. Suzuki, S. Kaneko, *J. Sol-Gel Sci. Technol.* **1998**, *12*, 87–94.
[13] Z. G. Wu, Y. X. Zhao, D. S. Liu, *Microporous Mesoporous Mater.* **2004**, *68*, 127–132.
[14] O. Stachs, V. Petkov, Th. Gerber, *J. Appl. Crystallogr.* **1997**, *30*, 670–674.
[15] D. R. Rolison, *Science* **2003**, *299*, 1698–1701.
[16] H. J. M. Bosman, E. C. Kruissink, J. Van der Spoel, F. Van der Brink, *J. Catal.* **1994**, *148*, 660–672.
[17] J. B. Miller, S. E. Rankin, E. I. Ko, *J. Catal.* **1994**, *148*, 673–682.
[18] J. R. Sohn, H. J. Jang, *J. Mol. Catal.* **1991**, *64*, 349–360.
[19] X. Gao, J. L. G. Fierro, I. E. Wachs, *Langmuir* **1999**, *15*, 3169–3178.
[20] Z. Dang, B. G. Anderson, Y. Amenomiya, B. A. Morrow, *J. Phys. Chem.* **1995**, *99*, 14437–14443.
[21] C. Contescu, *J. Catal.* **1995**, *157*, 244–258.
[22] G. Wang, X. Wang, S. Yu, *Stud. Surf. Sci. Catal.* **1994**, *83*, 67–74.
[23] M. K. Dongare, P. Singh, P. Moghe, P. Ratnasamy, *Zeolites* **1991**, *11*, 690–693.

[24] B. Rakshe, V. Ramaswamy, S. G. Hegde, R. Vetrivel, A. V. Ramaswamy, *Catal. Lett.* **1997**, *45*, 41–50.
[25] A. Brait, M. E. Davis, *Appl. Catal., A* **2000**, *204*, 117–127.
[26] A. Tuel, S. Gontier, R. Teissier, *Chem. Commun.* **1996**, 651–652.
[27] S. Gontier, A. Tuel, *Appl. Catal., A* **1996**, *143*, 125–135.
[28] D. J. Jones, J. Jiménez-Jiménez, A. Jiménez-López, P. Maireles-Torres, P. Olivera-Pastor, E. Rodriguez-Castellón, J. Rozière, *Chem. Commun.* **1997**, 431–432.
[29] A. Tuel, *Microporous Mesoporous Mater.* **1999**, *27*, 151–169.
[30] M. S. Morey, G. D. Stucky, S. Schwarz, M. Fröba, *J. Phys. Chem. B* **1999**, *103*, 2037–2041.
[31] M. L. Occelli, S. Biz, A. Auroux, *Appl. Catal., A* **1999**, *183*, 231–239.
[32] K. Chaudhari, R. Bal, T. K. Das, A. Chandwadkar, D. Srinavas, S. Sivasanker, *J. Phys. Chem. B* **2000**, *104*, 11066–11074.
[33] X. X. Wang, F. Lefebvre, J. Patarin, J. M. Basset, *Microporous Mesoporous Mater.* **2001**, *42*, 269–276.
[34] B. L. Newalkar, J. Olanrewaju, S. Komarneni, *J. Phys. Chem. B* **2001**, *105*, 8356–8360.
[35] M. S. Wong, H. C. Huang, J. Y. Ying, *Chem. Mater.* **2002**, *14*, 1961–1973.
[36] J. El Haskouri, S. Cabrera, C. Guillem, J. Latorre, A. Beltrán, D. Beltrán, M. D. Marcos, P. Amorós, *Chem. Mater.* **2002**, *14*, 5015–5022.
[37] X.-X. Wang, L. Veyre, F. Lefebvre, J. Patarin, J.-M. Basset, *Microporous Mesoporous Mater.* **2003**, *66*, 169–179.
[38] A. Infantes-Molina, J. Mérida-Robles, P. Maireles-Torres, E. Finocchio, G. Busca, E. Rodríguez-Castellón, J. L. G. Fierro, A. Jiménez-López, *Microporous Mesoporous Mater.* **2004**, *75*, 23–32.
[39] S.-Y. Chen, L.-Y. Jang, S. Cheng, *Chem. Mater.* **2004**, *16*, 4174–4180.
[40] C. Flego, L. Carluccio, C. Rizzo, C. Perego, *Catal. Commun.* **2001**, *2*, 43–48.
[41] G. J. A. A. Soler-Illia, C. Sanchez, B. Lebeau, J. Patarin, *Chem. Rev.* **2002**, *102*, 4093–4138.
[42] A. Tarafdar, A. B. Panda, P. Pramanik, *Microporous Mesoporous Mater.* **2005**, *84*, 223–228.
[43] J. W. Kriesel, M. S. Sander, T. Don Tilley, *Adv. Mater.* **2001**, *13*, 331–335.
[44] G. J. A. A. Soler-Illia, E. L. Crepaldi, D. Grosso, C. Sanchez, *J. Mater. Chem.* **2004**, *14*, 1879–1886.
[45] S. Cabrera, J. El Haskouri, C. Guillem, J. Latorre, A. Beltrán, D. Beltrán, M. D. Marcos, P. Amorós, *Solid State Sci.* **2000**, *2*, 405–420.
[46] P. Amorós, A. Beltrán, D. Beltrán, S. Cabrera, J. El Haskouri, M. D. Marcos, Patent WO 01-72635.
[47] T. R. Pauly, Y. Liu, T. J. Pinnavaia, S. J. L. Billinge, T. P. Rieker, *J. Am. Chem. Soc.* **1999**, *121*, 8835–8842.
[48] J. El Haskouri, D. Ortiz de Zárate, C. Guillem, J. Latorre, M. Caldés, A. Beltrán, D. Beltrán, A. B. Descalzo, G. Rodríguez, R. Martínez, M. D. Marcos, P. Amorós, *Chem. Commun.* **2002**, 330–331.
[49] J. El Haskouri, D. Ortiz de Zárate, F. Pérez-Pla, A. Cervilla, C. Guillem, J. Latorre, M. D. Marcos, A. Beltrán, D. Beltrán, P. Amorós, *New J. Chem.* **2002**, *26*, 1093–1095.
[50] M.-C. Chao, H.-P. Lin, C.-Y. Mou, B.-W. Cheng, C.-F. Cheng, *Catal. Today* **2004**, *97*, 81–87.
[51] S. Cabrera, J. El Haskouri, S. Mendioroz, C. Guillem, J. Latorre, A. Beltrán, D. Beltrán, M. D. Marcos, P. Amorós, *Chem. Commun.* **1999**, 1679–1680.
[52] S. Cabrera, J. El Haskouri, J. Alamo, A. Beltrán, D. Beltrán, S. Mendioroz, M. D. Marcos, P. Amorós, *Adv. Mater.* **1999**, *11*, 379–381.
[53] S. Cabrera, J. El Haskouri, A. Beltrán, D. Beltrán, M. D. Marcos, P. Amorós, *Solid State Sci.* **2000**, *2*, 513–518.
[54] J. El Haskouri, S. Cabrera, M. Gutierrez, A. Beltrán, D. Beltrán, M. D. Marcos, P. Amorós, *Chem. Commun.* **2001**, 309–310.
[55] J. El Haskouri, S. Cabrera, M. Caldés, C. Guillem, J. Latorre, A. Beltrán, D. Beltrán, M. D. Marcos, P. Amorós, *Chem. Mater.* **2002**, *14*, 2637–2643.
[56] J. El Haskouri, S. Cabrera, C. J. Gómez-García, C. Guillem, J. Latorre, A. Beltrán, D. Beltrán, M. D. Marcos, P. Amorós, *Chem. Mater.* **2004**, *16*, 2805–2813.
[57] R. K. Iler, *The Chemistry of Silica – Solubility, Polymerization, Colloid and Surface Properties, and Biochemistry*, John Wiley & Sons, New York, **1979**.
[58] S. A. Greenberg, D. Sinclair, *J. Phys. Chem.* **1955**, *59*, 435–440.
[59] C. F. Baes, R. E. Mesmer, *The Hydrolysis of Cations*, Wiley, New York, **1976**.
[60] D.-Y. Shin, S.-M. Han, K.-N. Kim, *J. Ceram. Processing Res.* **2004**, *5*, 70–75.
[61] N. Nishiyama, H. Saputra, D.-H. Park, Y. Egashira, K. Ueyama, *J. Membr. Sci.* **2003**, *218*, 165–171.
[62] L. Chu, M. I. Tejedor-Tejedor, M. A. Anderson, *Microporous Mater.* **1997**, *8*, 207–213.
[63] I. C. Tilgner, P. Fischer, F. M. Bohnen, H. Rehage, W. F. Maier, *Microporous Mater.* **1995**, *5*, 77–90.
[64] C. T. Kresge, M. E. Leonowicz, W. J. Roth, J. C. Vartuli, J. S. Beck, *Nature* **1992**, *359*, 710–712.
[65] L. Huerta, C. Guillem, J. Latorre, A. Beltrán, D. Beltrán, P. Amorós, *Sol. State Sci.* **2005**, *7*, 405–414.
[66] G. Pacheco, E. Zhao, A. García, A. Sklyarov, J. J. Fripiat, *J. Mater. Chem.* **1998**, *8*, 219–226.
[67] R. A. Schoonheydt in *Characterization of Heterogeneous Catalysts* (Ed.: F. Delannay), Marcel Dekker, New York, **1984**.
[68] W. N. Delgass, G. L. Haller, R. Kellerman, J. H. Lunsford, *Spectroscopy in Heterogeneous Catalysis*, Academic Press, New York, **1979**.
[69] M. Andrianainarivelo, R. Corriu, D. Leclercq, P. H. Mutin, A. Vioux, *J. Mater. Chem.* **1996**, *6*, 1665–1671.
[70] J. Scherzer, *ACS Symp. Ser.* **1984**, *248*, 157–158.
[71] J. C. Groen, L. A. A. Peffer, J. A. Moulijn, J. Pérez-Ramírez, *Chem. Eur. J.* **2005**, *11*, 4983–4994.
[72] S. Brunauer, P. H. Emmett, E. Teller, *J. Am. Chem. Soc.* **1938**, *60*, 309–319.
[73] E. P. Barrett, L. G. Joyner, P. P. Halenda, *J. Am. Chem. Soc.* **1951**, *73*, 373–380.

Received: December 22, 2005
Published Online: April 21, 2006

